

institute for optical systems

annual report 2013

Foreword



Hochschule Konstanz University of Applied Sciences (HTWG) has been one of the first Universities of Applied Sciences that has clearly committed itself to applied research. Today, HTWG has positioned itself in the growing group of research active Universities of Applied Sciences, and is continuously striving for even greater excellence, visibility, and leadership.

The research institutes play an essential role in the overall research activities of HTWG. The Institute for Optical Systems (IOS) has been founded as one of three focus institutes in 2008, and has lived up to its mission and HTWG's expectation ever since.

Measuring the success of research is generally a difficult task. It becomes easy, however, for individuals and institutes alike that contribute to the scientific community in many different ways. The IOS clearly is such an institute. Its members have published their work in numerous high quality publications, they have acquired substantial amounts of external funding, and they have successfully led several doctoral candidates to their advanced degree, to name only the most obvious contributions. The institute's success has only been possible because of the enthusiasm of its members, and its tight integration with HTWG. Students have contributed to the research work on various levels, and the results have been fed into the members' teaching. In this sense, the IOS has demonstrated the importance of excellent applied research also as a means for high quality teaching, in particular on the graduate level.

I am proud to write these few lines of thanks and congratulations for the IOS and cordially wish the institute, but first and foremost its members, ongoing enthusiasm, thirst for knowledge, and success for the future.

A handwritten signature in black ink that reads "Oliver Haase". The signature is written in a cursive, flowing style.

Prof. Dr. Oliver Haase
Vice-President for Research, University of Applied Sciences Konstanz

Preface

The present report gives an overview over the research and development activities of the Institute for Optical Systems (IOS) Konstanz in the years 2012 and 2013. Our main fields of interest are image processing, computer graphics, optical metrology and light engineering, thus representing the fundamental disciplines of current optical technology. The focus on optical systems as a whole allows us to offer competent partnership to the local industry in all relevant aspects. The IOS was founded in April 2008 by four professors from three different faculties of the University of Applied Sciences at Konstanz and is led by Prof. Dr. Umlauf (director) and Prof. Dr. Franz (associate director).

The following project descriptions present ongoing activities mainly on a status report level. Most of the reports are written by students working on their diploma, bachelor, master or Ph.D. theses. They reflect the largely varying levels of content, practice and insight that are characteristic for an institution involved in academic education. Due to its interdisciplinary nature, research at the IOS combines approaches from optics, computer graphics, image and signal processing, metrology, light engineering and sensor technology typically resulting in optical systems on a prototype level, either in pre-phase research or in cooperation with local industry.

On the occasion of our annual report, we would like to thank all of our students and co-workers for their enthusiasm and dedication which makes our institute a great place to be. Special thanks go to our institute officers, Pascal Laube and Michael Grunwald, and to Jürgen Keppler for smoothly managing our day-to-day activities. We are also indebted to the administration and staff of the HTWG Konstanz for their help, especially president Dr. Carsten Manz and Prof. Dr. Oliver Haase, for their support and for continuing the start-up funding, and the faculties of Mechanical Engineering, Electrical and Information Engineering, and Computer Science with the deans Prof. Dr. Thomas Böttcher, Prof. Dr. Thomas Birkhölzer and Prof. Dr. Jürgen Neuschwander for their assistance. Furthermore we appreciate the support of the Institute for Applied Research (IAF) Konstanz, especially Prof. Dr. Horst Werkle and Dipl.-Ing. FH Andreas Burger.

Contents

Institute Profile	6
IOS Building and Location Plan	7
Institute Members	8
IOS Staff	9
External Fundings and Grants	10
Cooperations with Research Institutions and Industry	10
Theses and Student Projects	11
Publications	12
Research Activities	18
3d-VLC Extensions	19
3d Gesture Interaction using Quaternion Rotations	21
Curved Triangular Surface Patches	23
Learning Geometric Primitives	25
On-line CAD Reconstruction with Accumulated Means of Local Geometric Properties	27
On-line Reconstruction of CAD Geometry	29
Pixel-wise hybrid image registration on wood decors	31
Iodine based optical frequency references for applications in space	33
An ESA-candidate mission: SpaceTime Explorer and Quantum Equivalence Principle Space Test	35
Double Reflector Luminaire with homogeneous rectangular light distribution	37
Picometer and Nanoradian Heterodyne Interferometry	39

Institute Profile

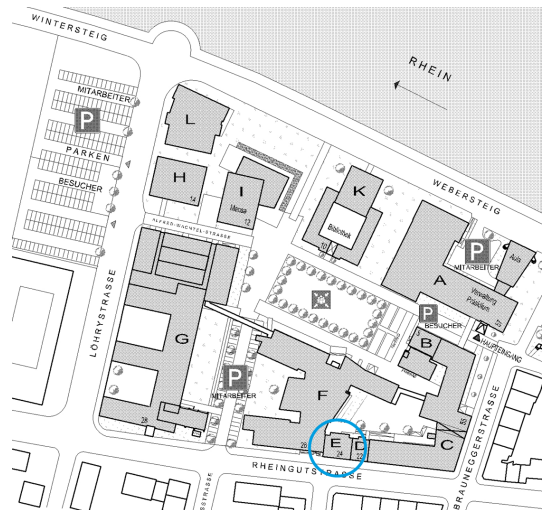


IOS BUILDING AND LOCATION PLAN



Institute for Optical Systems

Brauneggerstraße 55
Building E
3rd and 4th floor
78462 Konstanz



Location Plan

INSTITUTE MEMBERS

Prof. Dr. Georg Umlauf:



Diploma in computer science from University of Karlsruhe, 1996. Doctoral degree in computer science from University of Karlsruhe, 1999. PostDoc at University of Karlsruhe and University of Florida, Gainesville, USA, 1999-2000. Software development and senior researcher at Tebis AG, Hamburg, 2000-2002. Assistant professor for geometric algorithms at University of Kaiserslautern, 2002-2009. Interim professor for computer graphics at University of Karlsruhe, 2009. Since 2009 professor for computer graphics at University of Applied Sciences Konstanz and head of the computer graphics lab. Since 2010 member of the 'Institute for Optical Systems (IOS)' and 'Institute for Applied Research (IAF)'. Main research interests: Computer graphics, geometric modeling (splines, subdivision), reverse engineering, physical simulations.

Prof. Dr. Matthias Franz:



M.Sc. in Atmospheric Sciences from SUNY at Stony Brook, Diploma in physics from the Eberhard-Karls-Universität, Tübingen and doctoral degree in 1998. Thesis research in visual insect and robot navigation at the MPI for Biological Cybernetics and as a PostDoc at the Australian National University in Canberra. In industry he worked on various aspects of autonomous vision systems. 2002, he returned to the MPI as a group leader in the area of machine learning and computer vision. Since 2007 professor at the University of Applied Sciences in Konstanz and head of cognitive systems lab. Member of 'Institut für Angewandte Forschung (IAF)'. Main research activities in the development of automatically generated vision systems, optimisation and probabilistic modeling, with applications in industrial machine vision, texture analysis and steganalysis.

Prof. Dr. Claus Braxmaier:



Diploma in precision engineering at University of Applied Sciences Furtwangen. Diploma in physics and doctoral degree at the University of Konstanz in the field of fundamental tests of physics. Post-Doc at University of Konstanz. At EADS Astrium GmbH, system responsible for scientific and earth observation missions for ESA and head of group 'Mission Metrology'. Since 2005 professor for physics and control theory at the University of Applied Sciences Konstanz. Member of 'Institut für Angewandte Forschung' and 'Institut für Naturwissenschaften und Mathematik' Konstanz. Head of optical metrology research labs at HTWG and EADS Astrium GmbH. Main research: high resolution optical metrology for industrial and space applications.

Prof. Dr. Bernd Jödicke:



Study of physics at the University of Karlsruhe. Doctoral degree at Technical University Hamburg and University Karlsruhe in the field of high frequency technology. After that, industrial work at ABB Baden, Switzerland, as executive director for R&D. Since 1992 professor for applied physics at University of Applied Sciences Konstanz. Member of 'Institute for Applied Research (IAF)', 'Institut für Naturwissenschaften und Mathematik (INM)', 'Institute for Optical Systems (IOS) Konstanz' and 'Deutsche Lichttechnische Gesellschaft'. Head of laboratory for light engineering at HTWG. Main research activities in color and light measurements and color camera systems.

Prof. Dr. Burkhard Lehner:



Diploma in computer science from University of Kaiserslautern, 2004. Doctoral degree in computer science from University of Kaiserslautern, 2008. Software development at Sirona Dental System GmbH, Bensheim, 2008-2013. Since 2013 professor for computer science at University of Applied Sciences Konstanz. Since 2014 member of the 'Institute for Optical Systems (IOS)'. Main interests: software development, computational geometry, optical 3D measurement (especially in dental CAD/CAM).

Prof. Dr. Klaus-Dieter Durst:



Study of physics at the University of Stuttgart, 1986 doctoral degree in the field of magnetism at the Max-Planck-Institute of metal research. Thereafter research center Weissach of the Dr. Ing. h.c. F. Porsche AG, responsible for the central unit 'measurement technologies'. Since 1993 professor for measurement engineering and sensor technology at the University of Applied Sciences Konstanz. Member of 'Institut für Naturwissenschaften und Mathematik' and 'Institute for Optical Systems' Konstanz. Head of laboratories for measurement and sensor technology and production metrology. Currently director of 'Institut für Naturwissenschaften und Mathematik' Konstanz. Activities in the accreditation and surveillance of testing laboratories and inspection bodies.

IOS STAFF

Professors

Georg Umlauf, director IOS
Matthias Franz, associate director IOS
Claus Braxmaier
Bernd Jödicke
Burkhard Lehner
Klaus-Dieter Durst

Officer

Pascal Laube

Academic Staff

Markus Oswald
Markus Meßmer
Michael Grunwald
Johannes Stühler
Marco Fehrenbach
Jens Müller
Manuel Caputo
Rüdiger Schneider
Kai Brach
Daniel Scherz
Benjamin Dums

Postdoc

Thilo Schuldt

PhD Students

Klaus Denker
Jürgen Keppler
Roman Byshko
Pascal Laube
Dang Le
Ruven Spannagel

Student Assistants

Reiner Schlönvoigt
Benjamin Möllerke
Martin Miller
Korkiat Khumphai

EXTERNAL FUNDINGS AND GRANTS

- Amt für Städtebau, Stadt Zürich: Vorstudie Dendrochronologie. Entwurf eines Technologieschemas für einen hochauflösenden Scanner.
- ZAFH PHOTON[™] (European Union under EFRE and Baden-Württemberg funding); "Miniatur Lasersensor", 1 PhD student and equipment funds.
- Structure and Innovation Fund for Research, Baden-Württemberg, grant: "Automation and Communication", equipment funds.
- Baumer Inspection GmbH, Konstanz: "Farbtexturen in der industriellen Oberflächeninspektion", contract research.
- Baumer Inspection GmbH, Konstanz: "Inline - Inspektionstechnologie zum Farbgleich für den digitalen Dekordruck", contract research.
- DLR (Deutsches Zentrum für Luft- und Raumfahrt): "Langzeitstabile optische Frequenzreferenz auf Basis von molekularem Jod bei 532 nm (EBB mit EM-Design)", 1 Postdoc.
- Zentrales Innovationsprogramm Mittelstand, "Entwicklung eines technologisch völlig neuen, biometrischen Ganzkörper-Erkennungssystems auf Basis berührungslos, dynamisch erfasster 3d Signaturen", grant: 1 PhD student and equipment funds.
- Deutsche Forschungsgemeinschaft, "Laserunterstützte CAD-Konstruktion", grant: 1 PhD student and equipment funds.

COOPERATIONS WITH RESEARCH INSTITUTIONS AND INDUSTRY

Academic and Institutional Cooperations

- Humboldt-Universität zu Berlin
- ZARM (drop tower), Center of Applied Space Technology and Microgravity, Bremen
- DLR Institut für Raumfahrtssysteme Bremen
- University of Tübingen
- Max-Planck-Institute for Biological Cybernetics, Tübingen
- German Federal Office for Information Security (BSI), Bonn
- Universität Konstanz
- University of California, Davis
- Technische Universität Kaiserslautern
- University of Florida, Gainesville
- Grenoble Institute of Technology
- University of Strasbourg

Industry Cooperations

- EADS Astrium, Immenstaad
- Breuckmann GmbH, Meersburg
- Chromasens GmbH, Konstanz
- Baumer Inspection GmbH, Konstanz
- Procon-System GmbH, Thierstein
- Lightdesign-Solutions GmbH, Dresden
- Knotenpunkt, Wenzel Präzision GmbH, Balingen
- Tebis AG
- Liebherr Aerospace GmbH, Lindenberg
- NTT Data Deutschland GmbH
- Lacuna Solutions GmbH

THESES AND STUDENT PROJECTS

PhD Theses

- Andrew Paul Smith: Enclosure Methods for Systems of Polynomial Equations and Inequalities, Universität Konstanz, 2012.

Master Theses

- Matthias Greuter, Autonomous Mapping of Inland Waters using Radar Sensors, 2012.
- Sarbjit Kaur, Multiprocessor-Scheduling Simulator: Implementation & response time comparison of scheduling algorithms EDDP and SPA and resource protocol FMLP, 2012.
- Andreas Graumann, On the application of patch-based features to steganalysis, 2012.
- Siegfried Schneider, Adaptive Ausscheideregelung von Fremdpartikeln in Baumwolle, 2012.
- Hannes Hennig, Untersuchungen zur Umsetzung, Implementierung und Effizienz von Bildverarbeitungs- und Bildverbesserungsalgorithmen in einer GPU-basierten Hardware- und Softwareumgebung im Anwendungsfeld der Echtzeitbildverarbeitung, 2012.
- Samira Amiri, Entwicklung eines automatisierten Systems zur Mustererkennung in Felddaten aus Fahrzeugversuchen, 2012.
- Daniel Graf, Der Einfluss von Wasserzeichen auf die Steganalyse, 2012.
- Benjamin Dums, 3d Gestenerkennung, HTWG, 2012.
- Daniel Hagel, Online Reconstruction of Geometric Primitives, HTWG, 2012.
- Jakob Raible, Online Segmentation of Laser Scan Data, HTWG, 2012.
- Erich Buchmüller, Concept & prototypical implementation of a multplatform 3d viewer for displaying jt files on mobile devices, HTWG, 2013.
- Phillip Ziemer, Design and Implementation of a Multispectral Imaging System, Uni Konstanz, 2013.
- Markus Meßmer, Image Deconvolution, HTWG, 2013.
- Manuel Caputo, Learning geometric primitives in point clouds, HTWG, 2013.

Bachelor Theses

- Holger Strittmatter, Vermessung der dominanten Farben bei Dekordruck, 2012.
- Christoph Bender, Laser-Pointer-Steuerung eines Projektionssystems, HTWG, 2012.
- Manuel Caputo, 2d-Handgestenerkennung, HTWG, 2012.
- Rüdiger Scheider, 3d Particle-System with physical interaction using C#/XBA, HTWG, 2012.
- Irina Vidinjova, Konstruierung und Modellierung von Sattelpads, HTWG, 2012.
- Uwe Dittus, Visualisierung und Stimulation von Softwaresystemen, HTWG, 2013.
- Marco Fehrenbach, Landschaftsmodellierung mit Hilfe von Softwareagenten, HTWG, 2013.
- Helena Lorenz, Rotationsinterpolation in der 3D-Gesten-Steuerung, HTWG, 2013.
- Korkiat Khumphai, Aufbau einer Pipeline für eine Multispektralkamera, HTWG, 2013.
- Olexandr Shamray, Untersuchung von Mehrklassen-Stützvektormaschinen zur Echtzeitklassifikation für ein optisches Inspektionssystem in der Möbelindustrie, HTWG, 2013.
- Daniel Fritz, Integration eines Farbzeilenkamera-basierten 3D-Scanners in ein Programmiersystem, HTWG, 2013.
- Marc Bumiller, Echtzeit-Klassifikation für ein optisches Inspektionssystem in der Baumwollindustrie, 2013.
- Julian Bayer, Vergleich von Synchronisationsprotokollen für Multiprozessor-Scheduling in Realzeitsystemen, 2013.

Student Projects

- Angela Denninger, Alexander Frank, Alexander Pomrenke, Ralf Pöschik, "Implementierung eines 3D Video Moduls für den VLC Media Player", HTWG, 2013.
- Fehrenbach, Marco and Bayer, Julian and Danczak, Robert and Schuckert, Felix, "Metadaten in Bildern", HTWG, 2012.
- Duy Thai Nguyen, Ivan Pogorelov, "Lernhilfe-App zur Bildverarbeitung", HTWG, 2013.
- Bug, Andreas and Caputo, Manuel and Schneider, Rüdiger and Gabele, Christian, "Erkennung von Geschwindigkeitsbeschränkungen in Bildern", HTWG, 2013.

Journal Papers

- Franz, M.O. and Yovel, Y. and Melcón, M.L. and Stilz, P. and Schnitzler, H.-U., "Systematische Merkmalsbewertung in komplexen Ultraschallsignalen mit Lernmaschinen", *Informatik-Spektrum* 35 (5), 348-353, 2012.
- Aguilera, Deborah and Ahlers, H. and Battelier, B. and Bawamia, A. and Bertoldi, A. and Braxmaier, Claus and others, "STE-QUEST - Test of the Universality of Free Fall using Cold Atom Interferometry", *Classical and Quantum Gravity*, ISBN ISSN 0264-938, 2013.

Conference Proceedings

- C. Bender, K. Denker, M. Friedrich, K. Hirt, G. Umlauf, "A hand-held laser scanner based on multi-camera stereo-matching", *Visualization of Large and Unstructured Data Sets, OpenAccess Series in Informatics (OASISs)*, 17: 123-133, 2012.
- M. Caputo, K. Denker, B. Dums, G. Umlauf, "3d hand gesture recognition based on sensor fusion of commodity hardware". *Mensch und Computer 2012*, Oldenbourg Verlag, 293-302, 2012.
- K. Denker, D. Hagel, B. Hamann, J. Raible, G. Umlauf, "On-line Reconstruction of 3d Geometry", *Symposium on Geometry Processing*, Tallinn, Estonia, 16.-18.07.2012.
- P. H. D. Le and M. O. Franz, "How to Find Relevant Training Data: A Paired Bootstrapping Approach to Blind Steganalysis", *4th IEEE International Workshop on Information Forensics and Security (WIFS 2012)*, 228-233, 2012.
- Schuldt, Thilo and Döringshoff, Klaus and Stühler, Johannes and Kovalchuk, Evgeny and Franz, Matthias and Gohlke, Martin and Weise, Dennis and Johann, Ulrich and Peters, Achim and Braxmaier, Claus, "A Compact High-Performance Frequency Reference for Space Applications", *29th International Symposium on Space Technology and Science (ISTS 2013)*, Nagoya (Japan), 2013.
- K. Denker, D. Hagel, J. Raible, G. Umlauf, B. Hamann, "On-line reconstruction of CAD geometry.", *International Conference on 3d Vision*, IEEE, 2013, 151-158.
- K. Denker, D. Hagel, J. Raible, G. Umlauf, B. Hamann, "On-line reconstruction of CAD geometry.", *International Conference on 3d Vision*, IEEE, 2013, 151-158.
- P. H. D. Le, D. Graf, and M. O. Franz, "Steganalysis in the Presence of Watermarked Images", *Proceedings of the ninth International Conference on Intelligent Information Hiding and Multimedia Signal Processing (IIH-MSP-2013)*, 2013.

Conference Talks without Proceedings

- K. Denker, G. Umlauf, Online Reconstruction of 3d Geometry, *Eighth International Conference on Mathematical Methods for Curves and Surfaces*, Oslo, June 28 - July 3, 2012.
- K. Denker, G. Umlauf, 3d hand gesture recognition based on sensor fusion of commodity hardware, *Mensch und Computer*, Konstanz, 9.-12.9.2012, 2012.
- Klaus Denker: "On-line Reconstruction of 3d Geometry" *19th IMACS World Congress 26?30. August 2013*, Madrid.
- Klaus Denker, "On-line Reconstruction of 3d Geometry", *2013 SIAM Conference on Geometric and Physical Modeling*, 11-14. November 2013, Denver.

Poster Presentations

- K. Denker, D. Hagel, B. Hamann, J. Raible, G. Umlauf, "On-line Reconstruction of 3d Geometry", Symposium on Geometry Processing, Tallinn, Estonia, 16.-18.07.2012.
- K. Denker, D. Hagel, J. Raible, G. Umlauf, B. Hamann, "On-line reconstruction of CAD geometry.", International Conference on 3d Vision, 29/30. Juni 2013.

3d Laboratory

The IOS 3d Laboratory is split into two parts which are located in buildings F and E of HTWG and are led by Prof. Georg Umlauf. The 3d laboratory infrastructure mainly consists of devices for 3d capture and visualization.

A 3d projection system based on circularly polarized Sanyo XWGA projectors is able to create a 3d display for large audiences. The projectors have a resolution of 1280x800 and a brightness of up to 5.000 Lumens.

The Faro Edge 3d ScanArm is a handheld laser scanner that is able to capture 3d data of real life objects. The Scanner is able to capture data points with an accuracy of $\pm 25 \mu m$. Further capture devices include multiple Microsoft Kinects as well as a multi-camera stereo-matching system that can be used for realtime face reconstruction. All of the 3d Laboratory's workstations are equipped with high performance graphics cards.



Image Sensor Laboratory

The Image Sensor Laboratory is located in building E of HTWG and is led by Prof. Matthias O. Franz. It is used to build, evaluate and calibrate the various camera systems used in the image processing projects of the IOS.

Preliminary experiments are run directly in the IOS main office in a laboratory section which can be isolated with a light-proof curtain, whereas higher precision experiments are done in various laboratories on the HTWG campus with appropriate facilities. For high-resolution multispectral imaging, we dispose of a Peltier-cooled pco.4000 14 bit camera with a 4008×2672 CCD array and a VariSpec Tunable Filter that allows for selecting an arbitrary 30 nm wide band in the visual range via a computer interface.

For inspecting and processing colour images, we use a specialised graphics workstation with a high-fidelity calibrated colour display. Spectral measurements are done with a KonicaMinolta CS 2000 absolute spectrometer.

In applications requiring high CCD sensor sensitivities (such as the optical radar project), we have another Peltier-cooled pco.1600 colour camera with a 1200×1600 CCD array, but higher sensitivity.

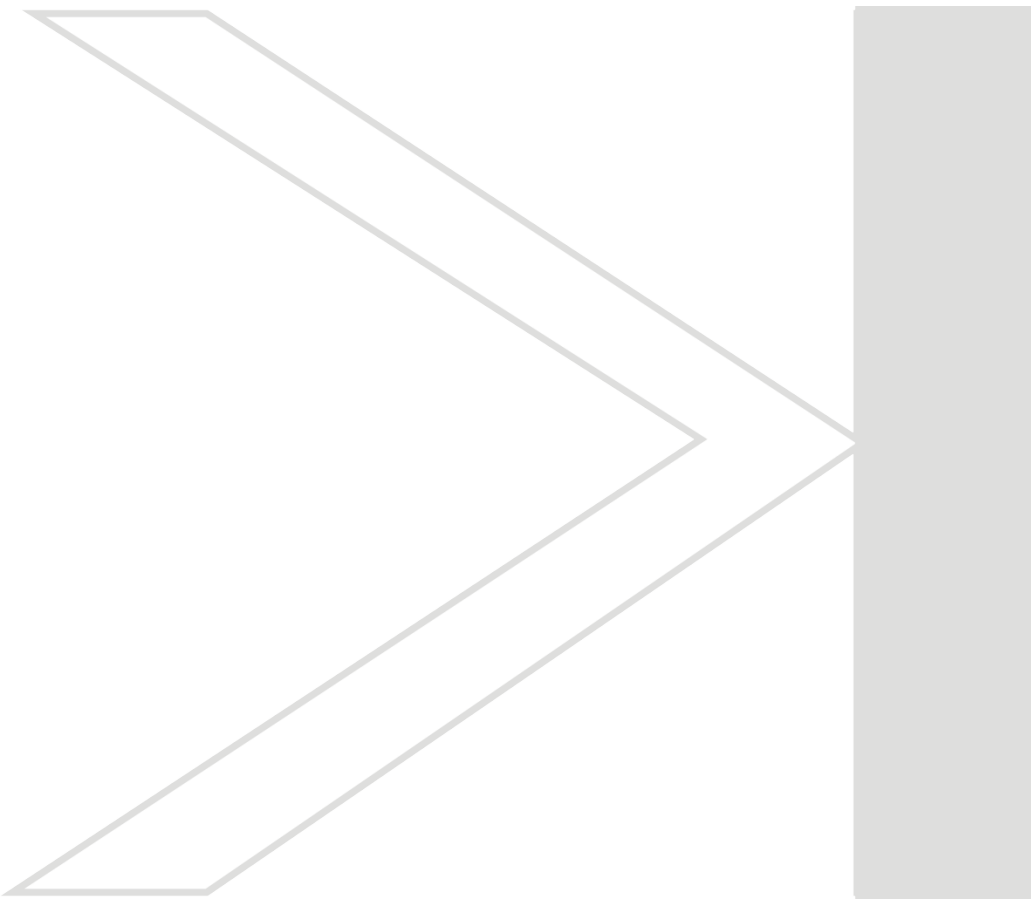


Computing Infrastructure



The compute and network environment of the institute is based on Intel and AMD multicore architectures connected with 1 GBit Ethernet. The 20 workstations use the operating systems Ubuntu Linux, Microsoft Windows and Mac OS. The central file server is integrated in the cluster system. For computation-intensive applications, such as multi-spectral image processing or the training of learning machines, we run a compute cluster under Ubuntu Linux. The cluster consists of a master node and a compute node with Intel Xeon CPUs, providing 40 processor kernels and 256 GB of RAM. Both nodes are mounted in a liquid-cooled rack with a 10 kW UPS. The internal cluster communication uses 2 GBit Ethernet and connects via FibreChannel to a RAID 6 storage system with 3.5 TB capacity to guarantee a high data throughput. Resources are managed with the SUN GridEngine. The cluster is connected to the backbone of the HTWG network via 10 GBit FibreChannel. Data backup is guaranteed by the central computer services of the HTWG.

Research Activities



3d-VLC Extensions

Angela Denninger, Alexander Frank, Alexander Pomrenke, Ralf Pöschik, and Georg Umlauf

One of the central tasks of the computer graphics group over the last years was to update and maintain the computer graphics laboratory in room F033 and improve its 3d interaction and visualization equipment and capabilities. The computer graphics laboratory houses a variety of visualization and interaction technologies, such as student workplaces for computer graphics programming, 3d projection based on polarization, GPU computation power, and various optical sensors. These hardware and software components had to be maintained, calibrated, improved, and configured. The core of the system is a 3d projection and interaction system for teaching, demonstration, visualizations, and research.

Introduction

Over the last year 3d technology advanced further and 3d movies have gain much mainstream interest. 3d visualization devices for the end user have become affordable and the number of available 3d media has risen considerably. However, there is up to day no open-source player for 3d media available, supporting the usual 3d data formats and visualization techniques.



Figure 1: The two projectors for 3d projection with the polarizing filters.

The computer graphics lab is equipped with a 3d projection system based on circularly polarized LCD projectors. This system has been developed at the HTWG. The technical setup is shown in Figure 1. For this system an open-source 3d media player was developed in this project. The basis for this project was the open-source media player VLC, that supports basically all known 2d media formats. The main goal of this project was an extension of the VLC player to support the most prevailing 3d media formats for images and videos. Furthermore, all 3d visualization techniques must be supported. The usual image and video codecs provided by the VLC player could be used for decoding.

3d extensions to the VLC player

In this project the multi-media player VLC was extended to support 3d functionality. This involves two different developments, for the input and the output of the player:

Input: For 3d image and video encoding every frame contains two frames, the so-called half-images. In order to encode these two highly correlated images efficiently, the image data is either interlaced (row-wise, column-wise or in a checkerboard pattern) or simply concatenated (side-by-side, top-bottom or rotated side-by-side), see Figure 2. Note that for all methods the resolution of both half-images is just half the resolution of the total frame. Thus, for visualization missing data needs to be interpolated.

After combining the two half-images to one image, they are encoded using the usual image or video codecs, e.g. jpg or mpg.

Output: For the stereoscopic output the half-images must be separated and streamed to the respective output channels for the individual eyes. This can again be interlaced in one output frame (e.g. for stereoscopic monitors based on polarization), overlaid in the same output frame (e.g. for anaglyphs), alternated in two subsequent output frames (e.g. shutter glasses), or concurrently in two synchronous output frames (e.g. polarized projection systems).

Especially the latter 3d-output method poses technical problems since due to the standard double-buffering for each channel a quad-buffering must be developed. Additionally, for the special 3d projection system developed at the HTWG the green-color channels need to be swapped. For real

time output all components need to be implemented using the GPU processing power. All these 3d extensions are to be integrated into the VLC module system.

Future plans

For the future we plan to modify and optimize the 3d visualization system in several ways:

- The 3d extensions are planned to be included into the official VLC download.
- Automatic input format detection.
- Implementation of a software lens correction for the projectors.
- Change the system architecture to a server based system, such that the administration of the software system becomes easier.
- Use the GPU power of the master computer for massive parallel online reconstruction processes.
- Realize a spatial calibration to optimize the 3d-projection the viewer's relative pose and orientation.
- Installation of a surround sound system for improved immersion.

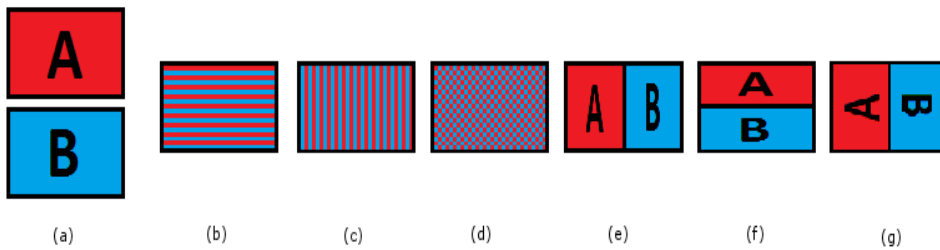


Figure 2: The different 3d media formats: (a) two half-images A and B, (b) row-interlaced, (c) column-interlaced, (d) checkerboard-interlaced, (e) side-by-side, (f) top-bottom, and (g) rotated side-by-side.

3d Gesture Interaction using Quaternion Rotations

Helena Lorenz, Klaus Denker, and Georg Umlauf

With the advent of various video game consoles and tablet devices gesture recognition got quite popular to control computer systems. E.g. touch screens allow for an intuitive control of small 2d user interfaces with finger gestures. For interactive manipulation of 3d objects in a large 3d projection environment a similar intuitive 3d interaction method is required. In a former project, we developed a dynamic 3d hand and arm gesture recognition system using commodity hardware. The input data was captured with low cost depth sensors (e.g. Microsoft Kinect) and HD color sensors (e.g. Logitech C910). The method combines dynamic hand and arm gesture recognition based on the depth sensor with static hand gesture recognition based on the HD color sensor. In this project, the rotation metaphor is enhanced. A representation of a rotation using homogeneous 4×4 -matrices is relatively un-robust near the so-called gimbal lock. Furthermore, interpolation of orientations in the matrix representation exhibit non-constant angular velocities. A more robust representation for rotations is given by quaternions. They do not have a gimbal lock and can be interpolated uniformly using SLERPs.

Introduction

User interfaces have changed a lot in recent years. Especially touch based interaction has become a common method to operate mobile phones and tablet PCs. However, touch screens have several problems. The finger touch leaves fingerprints on the screen, some on-screen content is occluded by the fingers, and for large displays (e.g. display size 2×3 meters) some display regions are inaccessible.

For 3d applications the biggest disadvantage is the limitation to two dimensions. Here, 3d gesture tracking allows a much more direct interaction with 3d objects. For a large projector system for 3d visualizations current interaction metaphors like mouse, keyboard, touch screens, or Wii Remote are either unfeasible or cumbersome to use. A direct 3d gesture interaction for this system is much more convenient.

With the Microsoft Kinect a low cost 3d camera is available to capture data at interactive frame rates but rather low resolutions at large distances. To increase the size of the operating space and the resolution we combined it with high-resolution web-cams in a former project, see Figure 3. The graphical user interface of this system is shown in Figure 4.



Figure 3: Sensor unit with a Kinect and a Logitech C910 web-cam.

Representation of rotations

The focus of the former project was on sensor fusion, arm gesture recognition and hand gesture recognition in three-dimensional object space. For the interaction metaphors only a very basic implementation was used. Especially for rotations this poses several problems. Using a matrix representation for rotations has several drawbacks.

- The matrix representation of rotations is based on so-called Euler angles. These are three angles around predefined axes that suffice to describe any rotation uniquely. However, if the of the axes get aligned on degree of freedom is lost, i.e. the rotation gets locked and the user cannot get out of this locked position. This phenomenon is called gimbal lock and is an intrinsic problem using any set of three angles to represent an arbitrary rotation in matrix form.
- For an arbitrary motion in 3d-space often only the start and end pose and orientation are given. The intermediate poses and orientations need to be interpolated. For the interpolation of the pose often linear interpolation is sufficient, resulting in a simple translation. For the interpolation of the orientation linear interpolation leads to non-constant speed along the trajectory.

Quaternions are one approach to overcome both problems of matrix representation of rotations. Quaternions are hyper-complex numbers with one real and three imaginary components. They have a standard component-wise addition and multiplication related to the scalar product and inner product of 3d-vector of the imaginary

components. The algebraic structure of quaternions is a non-commutative ring. The space of quaternions is four-dimensional and thus does not exhibit a gimbal lock.

Furthermore, using a suitable formulation of linear interpolation in the space of quaternions the resulting orientations yield a uniform distribution. This technique is known as SLERPs [Shoemaker85]. Therefore, using SLERPs the orientation changes uniformly with constant speed along a trajectory. With this approach any intermediate orientation represented by quaternion $q(t)$ at time $t \in [0, 1]$ can be computed from the start orientation q_s and end orientation q_e via

$$q(t) = \frac{q_s \sin((1-t)\theta) + q_e \sin(t\theta)}{\sin \theta},$$

with $\cos \theta = q_s * q_e$ and the 4d-scalar-product $*$.

Quaternion rotation results

The major goal of the project was to replace the rotation metaphor with quaternion rotations.

From the detected hand positions a axis of rotation and start & end hand poses & orientations are estimated. These yield the necessary quaternions

for the rotation and the SLERP construction.

Both methods are integrated to the prototypical 3d interaction system, see Figure 4. The resulting rotation metaphors are more robust and smoother for the user.

Future plans

For the future we plan to modify and optimize the 3d interaction system in several ways:

- Remove matrix operations altogether.
- Use an GPU implementation to speed up the affine transformations.
- Replace the interaction modes using a fuzzy approach to detect the dominant affine transformation and lock it.
- Use fuzzy approach for free-hand rotations, in order to lock the axis of rotation during manipulation. This is to enhance robustness, stability, and usability of the method.
- In the overall gesture interaction system replace the hand-detection by a glove-free approach.

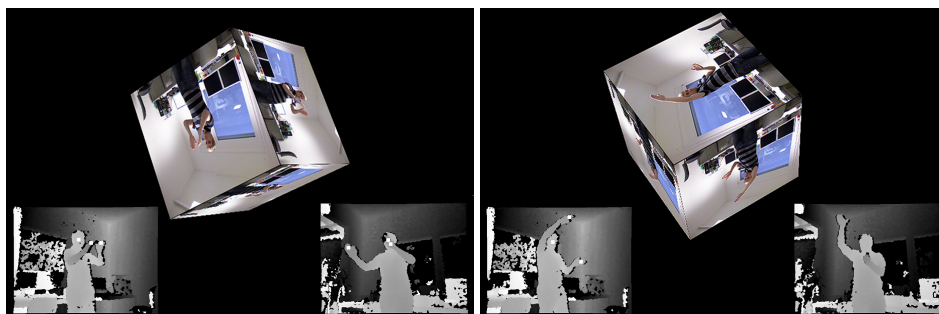


Figure 4: Rotation of a simple 3d scene using the demo application for 3d interaction.

Curved Triangular Surface Patches

Angela Denninger, Christian Badura¹, Alexander Muthler¹, and Georg Umlauf

Often CAD models are represented by triangle meshes. This is due to the simple geometry of triangles, efficient algorithms to generate triangle meshes from point clouds and efficient compression methods for triangle meshes. However, to generate triangle meshes that guarantee certain accuracy measures the number of necessary triangles increases significantly for highly curved geometries.

An alternative geometry representation in highly curved regions could be to use curved instead of planar triangles. In this project suitable triangle patch constructions were implemented and tested for their effectiveness in triangle meshes.

This project was in cooperation with tebis AG, Gräfelfingen.

Introduction

A standard problem in CAD and CAGD is how to represent a 3d model with a minimal number of data points (vertices) while guaranteeing at the same time the structure of the model and certain quality measures. This is particularly important for highly curved regions and models containing sharp features.

Two standard representations are here splines or triangle meshes. While splines can represent curved geometry highly accurate, they usage implies global smoothness constraints. These constraints complicate the constructions and processing. On the other hand, triangle meshes are the simplest representation for 3d geometry, guaranteeing accuracy might increase the amount of required data significantly. In order to guarantee a certain accuracy in a highly curved region the size of the triangles must shrink. At the same time number of triangles is increased, rendering the use of triangle meshes sometimes impractical.

In this project a combination of both approaches is analyzed. Starting from a high resolution triangle mesh that satisfies approximation properties, the number of triangles in curved regions shall be reduced using curved triangles instead of planar ones. This means, that triangles must be combined based on an appropriate error measure. These curved triangles are represented as polynomial or rational splines. Incorporating additional local smoothness constraints can further reduce the error allowing for a larger reduction of the number of triangles.

Thus, the focus of this project was on a comparison of different triangle patch constructions, suitable combination strategies, and appropriate error measure.

¹Tebis AG, Gräfelfingen

Project requirements

In order to fulfill the technical requirements of industrial CAD modeling tools, a set of requirements for the triangle patch construction can be identified:

1. Sharp features must be preserved..
2. In the absence of sharp features, adjacent triangle patches must maintain G^1 -smoothness across their common boundary.
3. Various approaches need to be evaluated. Thus, there is the need for easy exchange of methods.
4. The representation must be suitable for further processing.
5. The representation is based on existing high resolution triangle meshes.
6. The representations must allow for an efficient evaluation of the respective error measures.

Among the numerous triangle patch constructions in the literature, cubic WM-triangles of [Waton, Meek 1996] and PNG1-triangles of [Fünzig et al. 2008] fulfill these requirements best and were implemented.

Hierzu werden im Rahmen dieser Thesis PNG1 Dreiecke und kubische Walton und Meek Dreiecke als Approximationsverfahren verwendet.

Results and future plans

Since the original CAD geometries were represented as high resolution meshes the used error

measure was an edge-based sampling error. Especially along sharp features this is the most important measure. Using also normal information along these sharp features might lead to further improvements.

For the combination strategy topological entities in the triangle mesh need to be collapsed. Here the standard approach of edge collapses was used. An edge collapse yields immediately the two triangles to combine. Furthermore, this approach allows for a greedy collapsing strategy using the anticipated edge error along the collapsed edge. However, since edges in a triangle mesh are the defining entities for sharp features, collapsing feature edges might lead to severe deformations of the shape of the model. Therefore, many special cases for feature edge collapses need to be developed, to yield significant compression close to features in the mesh.

In the comparison of the different methods curved triangle representations approximate the CAD model to a factor of two better than planar triangle meshes. This means that on average the number of triangles is halved. However, the absolute data reduction depends highly on the structure if the underlying geometry. For cylindrical shapes or medium curved geometries the two implemented triangle patches are best suited, see

Figure 5 and 6. For low curved regions or fillets the approximation power of the implemented triangle patches does not reduce data size sufficiently.

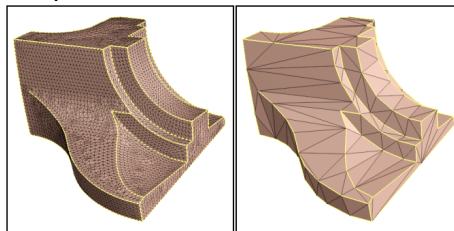


Figure 5: Results of the mesh optimization: left original mesh with 12.946 faces and right the optimized mesh with 200 faces.

For these reasons we plan for the future to extend the project in several ways:

- Evaluate more triangle patch constructions.
- Use an edge based error measure with normal information along sharp features.
- Use a surface based error measure.
- Use vertex or face collapses as triangle combination strategy.

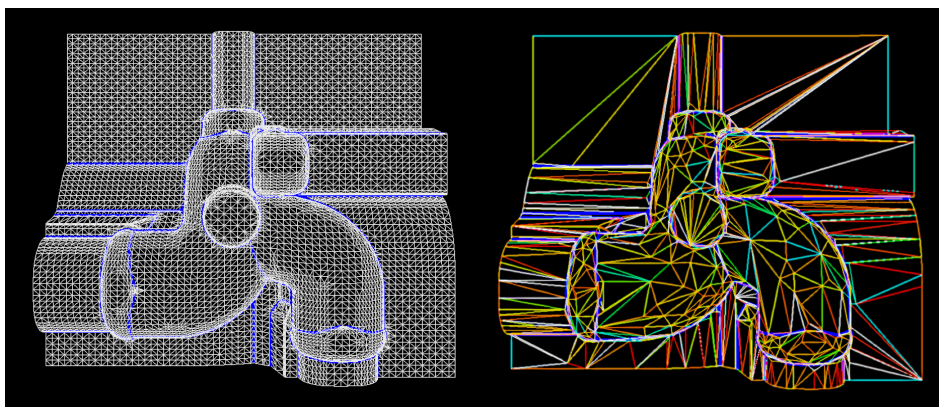


Figure 6: The original triangle mesh (left) with sharp features and the optimized mesh using Walton/Meek triangles (right).

Learning Geometric Primitives

Manuel Caputo, Klaus Denker, Matthias Franz, Pascal Laube, and Georg Umlauf

Primitive recognition in 3D point clouds is an important aspect in reverse engineering. We propose a method for primitive recognition based on machine learning approaches. The machine learning approaches used for the classification are linear discriminant analysis (LDA) and multi-class support vector machines (SVM).

For the classification process local geometric properties (*features*) of the point cloud are computed based on point relations, normals, and principal curvatures. For the training phase point clouds are generated using a simulation of a laser scanning device based on ray tracing with an error model. The classification rates of novel, curvature-based geometric features are compared to known geometric features to prove the effectiveness of the approach.

Introduction

The reconstruction of CAD data from 3D scans has become more important in the last years. An important part of this reconstruction process is the detection of geometric primitives such as planes or cylinders within the scanned components. Our method works directly on the raw point cloud and does not require initial meshing. In [2] a system for online reconstruction is proposed, that uses a fixed set of heuristic rules for primitive detection based on estimation of local differential geometric properties. Since this system works only for planes, cylinders and spheres additional methods are required to detect other primitives such as cones or tori. Machine learning algorithms classify input samples and predict their class by learning to discriminate the different classes within certain feature spaces from training samples. These machine learning algorithms require fixed length feature vectors as input. We use pre-trained machine learning algorithms to label point cloud patches (Fig. 7) with their corresponding primitive class.

Machine Learning methods and feature extraction

Two machine learning algorithms were used. First tests were conducted using *Linear Discriminant Analysis* (LDA). Second, a *d*-class *Support Vector Machine* (SVM) was used for open and closed classification. Supervised learning methods are designed to classify new data with respect to a large body of pre-classified training data. The training data are represented as feature vectors which are chosen to separate the different classes from each other. To apply machine learning algorithms such as linear discriminant analysis (LDA) or support-vector machines (SVM) a training phase is re-

quired. In the training phase the LDA and SVM are exposed to a large set of pre-classified point clouds to learn to discriminate between the different classes. The information about these classes is implicitly represented in distributions of geometric features extracted from the local geometry in the point cloud. Acquiring real scanned point clouds for the training is difficult, because scanning a sufficiently large number of training point clouds would require a substantial amount of time and a large number of different real world models. These training point clouds are generated by a laser scanning simulation. This simulation is based on ray tracing to compute the intersections of a simulated laser line probe and a virtual geometric primitive. It simulates the behavior of real laser scanners by sweeping fans of light rays from a scan position over the geometric primitive.

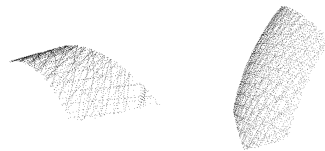


Figure 7: Point cloud patches of a cylinder (left) and a sphere (right).

The laser scanner model includes two types of systematic errors: A random offset added to the scanner position and to each scanned point.

Model selection refers to the process of selecting the best parameters for the SVM. For this optimization usually a grid search in the two-dimensional space is used. We used a two-dimensional non-uniform grid on which all pairwise parameter combinations are evaluated. To compare the different models, *k*-fold cross validation is used. To better understand the classification properties of individual SVMs the separating

hyper-surfaces are visualized. Fig. 8 shows some examples of hypersurfaces of trained SVMs.

We testet several geometric features from the following which can be grouped by categories:

- Features that are only based on the location of the points in the point cloud.
- Normal-based features using point normals.
- Curvature based features using principal curvatures and curvature directions.

We also evaluated feature combinations from these three categories. The extracted features are arranged in histograms with 2^i bins, $i = 6, \dots, 9$. These histograms might be normalized and cropped to eliminate outliers. For the computation of the geometric features normals, principal curvatures and principal curvature directions at random points in the point cloud must be estimated. To estimate a local normal at a point in the point cloud a set of its closest neighbors is determined. Normal estimation is then done by computing a principal component analysis (PCA). To estimate the principal curvatures and principal

curvature directions at a point the polynomial fitting of osculating jets of Cazals and Pouget [1] is used.

Future work

For future work we intend to detail the pros and cons of various geometric features and their dependence on the distribution of the training data for SVM classification. To generate simulated scans that match real scans as close as possible is another aspect we plan to investigate. Additionally we plan to extend the machine learning methods to multi-output SVMs to allow for a larger set of geometries to recognize.

Bibliography

- [1] Cazals, F. and Pouget, M.: Estimating differential quantities using polynomial fitting of osculating jets, *Computer Aided Geometric Design*, 22, 121–146, 2005.
- [2] Denker, K. and Hagel, D. and Raible, J. and Umlauf, G. and Hamann, B.: On-line Reconstruction of CAD Geometry, *Inter. Conf. on 3D Vision*, 151–158, 2013.

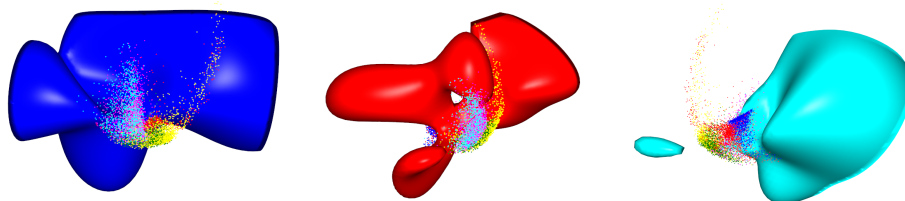


Figure 8: Separating hyper-surfaces of the SVM to classify planes (blue), cones (red), and spheres (cyan). Remaining points refer to cylinders (green), ellipsoids (magenta), and tori (yellow).

On-line CAD Reconstruction with Accumulated Means of Local Geometric Properties

Klaus Denker, Bernd Hamann, and Georg Umlauf

Reconstruction of hand-held laser scanner data is used in industry primarily for reverse engineering. Traditionally, scanning and reconstruction are separate steps. The operator of the laser scanner has no feedback from the reconstruction results. On-line reconstruction of the CAD geometry allows for such an immediate feedback.

We propose a method for on-line segmentation and reconstruction of CAD geometry from a stream of point data based on means that are updated on-line. These means are combined to define complex local geometric properties, e.g., to radii and center points of spherical regions. Using means of local scores, planar, cylindrical, and spherical segments are detected and extended robustly with region growing. For the on-line computation of the means we use so-called accumulated means. They allow for an on-line insertion and removal of values as well as merging of means.

Our results show that this approach can be performed on-line and is robust to noise. We demonstrate that our method reconstructs spherical, cylindrical, and planar segments on real scan data containing typical errors caused by hand-held laser scanners.

Introduction

We present an on-line algorithm for segmentation and reconstruction of CAD geometry from a stream of point data. Our approach is based on accumulated means of local geometric properties and classification scores for different surface types. Accumulated means allow for on-line insertion and removal of data and merging of means.

Current Status

The advantage of using means of geometric properties instead of purely local geometric properties for the detection of surface segments is the increased stability in the computations. Thus, we use means throughout our on-line approach.

For on-line computations means are computed by incremental addition of data. Besides, it is necessary to remove data from a mean or to merge two means. We call a quantity *accumulated* when it supports these three *accumulation operations*.

For each n -ball in a ball tree [1,2] we obtain sets of values that are combined in accumulated arithmetic means. Unweighted arithmetic means are used for position p , normal n , and ball radius r . Their means \bar{p} , \bar{n} , \bar{r} are used to detect planar segments. Accumulated weighted arithmetic means $\bar{\kappa}_1$, $\bar{\kappa}_2$, \bar{H} are computed for principal curvatures κ_1 , κ_2 , and mean curvature H . The respective weights used in the computation are given by the

quality score q_{ls} of the local least squares fit.

Accumulated means are also defined for normalized un-oriented vector-valued data, e.g., principal curvature directions. It is also possible to combine existing means with local data to new local geometric estimates, e.g. hypothetical cylinder and sphere center points.

Scores for geometric primitives s_{pln} , s_{cyl} , s_{sph} , and s_{ffg} are computed for segmentation. They provide the information how good a n -ball fits to an segment in the local neighborhood if it would have a certain segment type. Weighted means of the scores \bar{s}_{pln} , \bar{s}_{cyl} , \bar{s}_{sph} , \bar{s}_{ffg} are used to determine the type of segments. Segments with very similar accumulated means of their relevant geometric properties are merged.

For each segment a boundary is computed using an on-line boundary computation.

We use simulated scans of basic geometric primitives to evaluate the robustness of this method to noise. In Figure 9 the reconstruction quality of synthetic scans using real recorded hand movements is compared. The simulated plane has an edge length of 20 cm. The cylinder height is 20 cm and the radius is 10 cm; the sphere radius is 10 cm. The added noise is simulated using normal-distributed random numbers. It is scaled according to different levels of standard deviation σ .

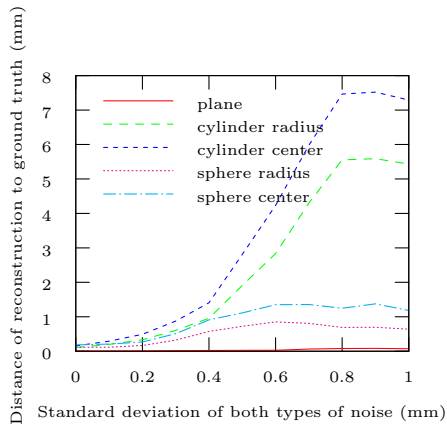


Figure 9: Plot of average distances of 25 experiments for noise levels $\sigma = i/10[mm]$, $i = 0, \dots, 10$, all segment types.



Figure 10: Reconstruction from a scan of the driver's cabin of a wooden fire truck toy: segments colored by segment type: **planar**, **cylindrical**, and **spherical**.

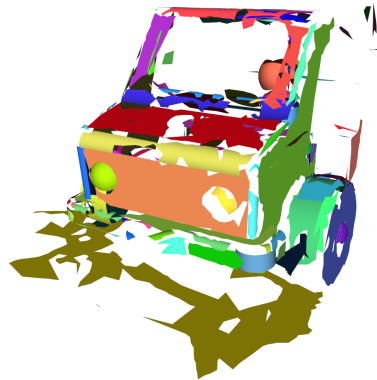


Figure 11: Reconstruction from a scan of the driver's cabin of a wooden fire truck toy: each segment colored individually.

Tests with real scan data are shown in Figures 10 and 11. The wooden toy fire truck was scanned with a *Faro Edge Laser Scan-Arm*. The shown scan consists of 1271342 points and 12325 scan lines. The reconstruction uses 15013 n-balls and results in 1011 segments.

Next Steps

Currently the approach is limited to planar, cylindrical, and spherical shapes. We plan to extend the approach to other geometric primitives like cones, ellipsoids, tori, and rolling ball blends.

The on-line boundary reconstruction needs to be improved.

Acknowledgments

This work was supported by DFG grants UM 26/5-1 and IRTG 1131.

Bibliography

- [1] K. Denker, B. Lehner, G. Umlauf: Online triangulation of laser-scan data, R. Garimella (ed.), Proceedings of the 17th International Meshing Roundtable, Springer, pp. 415–432, 2008
- [2] K. Denker, B. Lehner, G. Umlauf: Real-time triangulation of point streams, Engineering with Computers, 27(1): 67–80, 2011.

On-line Reconstruction of CAD Geometry

Klaus Denker, Daniel Hagel, Bernd Hamann, Jakob Raible, and Georg Umlauf

In reverse engineering and computer-aided design (CAD) applications point cloud data is usually manually scanned, reconstructed, and post-processed in separated steps. When point cloud data resulting from a scanning process do not satisfy certain necessary reconstruction requirements, one must perform scanning again to enable proper reconstruction. On-line reconstruction of 3d geometry allows one to generate and update a CAD reconstruction on-line during the scanning process with an hand-held laser scanner. Thus, regions where the scanned data is insufficient for the reconstruction are detected on the fly to allow an immediate correction and improvement of the scanned data. This enables the operator to focus on critical regions in the scanned data to improve the reconstruction quality.

We present an on-line segmentation and on-line reconstruction of basic geometric primitives. The presented methods allow for a real-time processing of a point stream. They utilize data structures that can be updated at any time when additional data from the stream has to be processed. This data is used to complete and improve the segmentation and reconstruction during the scanning process.

Introduction

Hand-held laser scanners are used in reverse engineering to sample the geometry of physical objects. Commercial software in this area only allows a point based preview of the scanned data. The geometry is reconstructed in a separate, post-processing step. Parameters of the geometry are manually extracted from the point or mesh data. If there is data missing for a successful reconstruction, the whole process will fail. The complete scanning and reconstruction process has to be repeated.

With an on-line reconstruction algorithm, the reconstruction is computed concurrently with the acquisition of the point data during the scanning process. Regions where data is missing for the reconstruction can be detected on the fly. The human operator of the laser scanner can immediately re-scan this region to improve the reconstruction. Additional data is added to all existing data structures to improve reconstruction constantly.

In this work, the focus is on on-line segmentation and on-line reconstruction of basic geometric primitives [3]. The current on-line reconstruction process is fully automated without user interaction except for the handling of the hand-held laser scanner. Specifically, the contribution is the development and implementation of a geometry reconstruction method that automatically generates a surface representation in real time from a stream of scanned point data.

Current Status

The basic data structure for the on-line reconstruction is a ball tree as described in [2]. This data structure stores and processes the data stream from the laser scanner and prepares it for all subsequent reconstruction steps.

	$K > \varepsilon_K$	$ K \leq \varepsilon_K$	$K < -\varepsilon_K$
$H < -\varepsilon_H$	 peak	 ridge	 saddle ridge
$ H \leq \varepsilon_H$	—	 plane	 minimal surface
$H > \varepsilon_H$	 pit	 valley	 saddle valley

Table 0.2: Eight surface types determined by the Gaussian and mean curvature [1].

For the segmentation of the scan data the n-balls are classified by their local geometry, see Table 0.2. Based on this classification, an on-line region growing algorithm is applied to obtain segments of the same surface type. This region growing is guided by segmentation criteria ensuring geometric consistency within segments. Based on the information about global surface segments the geometric classification is improved, see Figure 12.

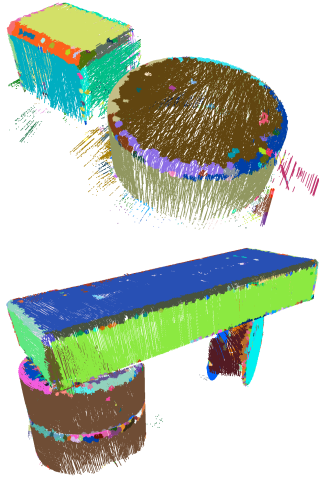


Figure 12: Resulting segments colored individually.

A boundary polygon for each segment is constructed using a modified alpha shapes approach.

Then, geometric primitives are reconstructed for each segment. In order to reduce the memory consumption and the complexity of the representation implicit quadrics are used, similar to [4]. Using this representation the set of n-balls for a segment can be reduced to a set of ten coefficients defining a quadric

$$0 = q(x) = x^T Q x + 2P^T x + R \quad \text{for } x \in \mathbb{R}^3$$

where

$$Q = \begin{bmatrix} A & D & E \\ D & B & F \\ E & F & C \end{bmatrix} \quad \text{and} \quad P = \begin{bmatrix} G \\ H \\ I \end{bmatrix}.$$

After the fitting the quadric surface is trimmed at the boundary polygon to yield a standard b-rep of the scanned points.

The canonical system of a quadric is given by the eigenvectors e_1, e_2, e_3 of Q . To get the correct translation of the quadric surface, the equation $Qx + P = 0$ is solved. The solution of this equation yields either a center point, a point on a centerline, or a point on a center plane. This yields a complete representation of the spatial position of the quadric surface.

Using the canonical system of the quadric and ray-casting, all parameters of the geometric primitives can be computed, see Figure 13.

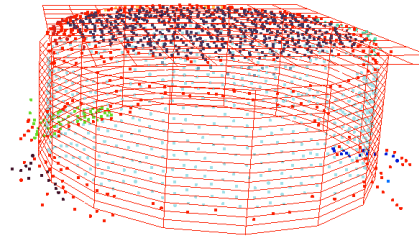


Figure 13: Geometric primitives reconstructed from a scan of a wooden cylinder.

Next Steps

Aspects for improvement of the on-line reconstruction process concern trimming and SVD computation. Primitives are currently not trimmed. The boundary polygons of the segments will be projected to the geometric primitives and used as trim curves. For the quadric fitting a SVD is used, where an on-line SVD method could improve the performance. Furthermore, the presented method is limited to surfaces that can be reconstructed by quadrics. Blends in CAD models may contain surface types that can not be reconstructed by quadrics, e.g., a monkey saddle. For these surfaces a more general surface representation is required.

Acknowledgments

This work was supported by DFG grants UM 26/5-1 and IRTG 1131.

Bibliography

- [1] P. J. Besl and R. C. Jain, Segmentation through variable-order surface fitting, *IEEE Transactions on Pattern Analysis and Machine Intelligence*, 10(2): 167–192, 1988.
- [2] K. Denker, B. Lehner, G. Umlauf: Real-time triangulation of point streams, *Engineering with Computers*, 27(1): 67–80, 2011.
- [3] K. Denker, D. Hagel, J. Raible, G. Umlauf, B. Hamann: On-line Reconstruction of CAD Geometry, *Proceedings of the International Conference on 3D Vision*, IEEE, pp. 151–158, 2013.
- [4] M. Vančo, B. Hamann, G. Brunnett: Surface reconstruction from unorganized point data with quadrics, *Computer Graphics Forum*, 27(6): 1593–1606, 2008.

Pixel-wise hybrid image registration on wood decors

Jens Müller, Matthias O. Franz, Michael Grunwald

This work deals with pixel-wise hybrid image registration of wood decors. A line scan camera takes two pictures of two different prints of the same wood decor. The first image is a reference image. The second one is the same image which has been printed out again. The aim was to match these images as precisely as possible using different software algorithms. First, the entire images are matched by calculating parameters for the transformation and applying these parameters to the one image. This is done by extracting feature points from both images and correlating them to each other. These parameters are calculated by using the extracted and correlated feature points as image and object points for the equation of the projective transformation. In order to avoid mismatched features, a RANSAC system is used. This system repeats the calculation with a different subset of input data until the result is above a given precision. In order to get a pixel-wise registration, local invariances within the images are considered, too. These invariances can occur if the line scan camera varies in speed, for example. An interpolation of the position of the matched feature points is done by using a Gaussian process and a thin plate splines algorithm.

Introduction

Nowadays, most wooden-looking furniture or floors are made of artificially printed wood decors instead of real wood. In order to ensure that the printed decors are of high quality and do not differ in colour, experts have to check the correct mixing ratio of the printing colours. The printed decors should not differ from the original. This thesis is part of a larger project which aims at creating a system that automatically detects difference in colour between a print and its original. The first step of the automated detection is the scanning of the original and the print with a line scan camera. If the original and the printed image are compared, only the corresponding pixels should be compared to each other. The master thesis introduces a prototype for the registration of images with wood structures with an accuracy of at least one pixel. The registration prototype is built in five steps:

1. Extraction of feature patches as image substitutes.
2. Correlation of these patches in both images.
3. Calculation of model parameters which describe the transformation of the images.
4. Validation of the quality of the model. Repetition of step 3 with a new subset of input pairs if the quality is not above a defined value.
5. Correction and interpolation between the features in order to improve the accuracy of the solution.

The first four steps are a global image registration solution. This means that one solution is found for the whole image and the same transformation is applied to all pixels. The last part of the solution can be considered a local registration as local parts of the image are transformed differently. The correction is done with a machine learning algorithm called a Gaussian process. Additionally, the thin plate spline interpolation algorithm is compared to the Gaussian process. This algorithm is one of the state of art algorithms for local interpolation between features. The developed prototype can be considered a hybrid system of both of these registration types.

System

This overview is an abstract description of the registration system. It consists of several parts. As a first step, the two images were read in. As a second step, the threshold for the extraction of the feature point algorithm were calculated. As a next step, feature areas were extracted from the image. This was done in order to receive a small set of data which represents the geometry of the entire image. For the calculation of the transformation, the feature areas had to be the same in both images. In order to know which areas on the one image corresponded to the areas on the other image, it was necessary to match the feature areas. This is why all feature areas were matched with the Pearson correlation coefficient. In order to avoid mismatches, the mapped areas were filtered after the matching. The correlated features were used to calculate the transformation parameters of a transformation model. These parameters describe the global transformation of the image. The image

could then be transformed considering the transformation model and the calculated parameters. The second part of the process was the local registration. The calculated global transformation was applied to the extracted feature points in order to receive the new image representation. At this point, the corresponding feature pairs should have been nearly at the same position. However, local differences in the scanned images occurred. These differences did not result from the imprecision of the features but may have resulted from the slightly varying speed of the line scan camera. This is why technologies for the local correction were examined. The transformations were corrected by interpolating between the feature points of the entire image. The first technology examined was a Gaussian Process. A Gaussian process learned the local transformation of the already globally correct feature points and made a prediction about local transformations for the entire image. Since this technology had not been used for the interpolation in local image registration before, it was compared to a state of the art interpolation algorithm, the thin plate splines. Thin plate splines are also a technology for interpolation, often used in the field of aerial photography.

Results

In order to get representative results for each calculation, the cross validation method was used. In this strategy, the feature points were divided into equal random subsets and all but one of them were used for the calculation of the solution. This solution was afterwards applied to the unused subset and the error of the result was calculated. The error was measured in the absolute value of pixel deviation of the transformed feature point on the untransformed feature point of all points in the

test set. This test was repeated for all subsets. The input images for the test were several wood decor motives with different transformation applied on. After the comparison of different algorithms for the extraction of features, the calculation of the transformation and the interpolation, the combination of blob extraction, perspective transformation and thin plate splines (Fig. 14) turned out to be the most precise.

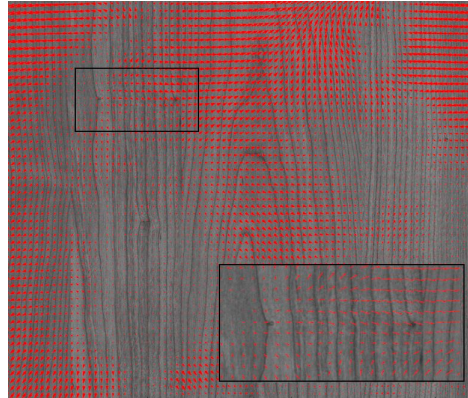


Figure 14: Transformation of the thin plate splines on a grid of points across the image.

The Gaussian process was intensively examined with different Kernels but was not as precise as the thin plate splines algorithm in average. The Gaussian process appeared to have stronger problems with areas of low contrast. In these areas no features could be extracted and therefore the interpolation was not as precise as the one of the thin plate splines. The combination of the best algorithms are able to calculate an average precision of at least 0.2 pixels in all test cases.

Iodine based optical frequency references for applications in space

Thilo Schuldt, Johannes Stühler, Klaus Döringshoff, Martin Gohlke, Dennis Weise, Ulrich Johann, Matthias Franz, Achim Peters, and Claus Braxmaier

Several future space missions require optical frequency references with a stability in the 10^{-15} domain at longer integration times. For this purpose, we developed two setups based on Doppler-free spectroscopy using molecular iodine. We built up and tested assemblies on elegant breadboard (EBB) and engineering model (EM) level, providing a frequency stability of $3 \cdot 10^{-15}$ at an integration time of 200 s. Main design drivers were compactness and thermal and mechanical stability. The setup on EM level was successfully subjected to vibration testing and thermal cycling.

Introduction

Future space missions related e.g. to fundamental science, earth observation and navigation and ranging require ultra-stable frequency references, especially in the optical domain. Lasers stabilized to atomic or molecular transitions offer an absolute frequency reference with high long-term frequency stability. Appropriate setups based on Doppler-free spectroscopy offer frequency stabilities in the 10^{-15} domain at longer integration times and have the potential to be developed space qualified in a relatively short period of time.

Optical frequency reference on EBB-level

We realized an ultra-stable optical frequency reference on elegant breadboard (EBB) level which utilizes modulation-transfer spectroscopy of molecular iodine near 532 nm. Compactness and mechanical and thermal stability were main design drivers as the development is carried out with respect to future applications in space. The setup on EBB level was built up on a baseplate made of Clearceram-Z HS, a glass ceramics with an ultra-low coefficient of thermal expansion (CTE) of $2 \cdot 10^{-8} \text{ K}^{-1}$. All components including the triple-pass iodine cell with a length of 30 cm, the mirrors, polarisers, beam-splitters and fibre-collimators are either directly, or by the use of special invar mounts, adhesive bonded to the baseplate. This setup allows for high long-term frequency stability due to enhanced pointing stability by using exclusively components with very low CTE and stable, quasi monolithic, mountings. A photograph of the EBB setup is shown in Fig. 15 where the interaction of laser beam and molecular iodine is visible. All optical elements are fixed

to the baseplate using adhesive bonding technology. The dimensions of the Clearceram baseplate are $550 \times 250 \times 50 \text{ mm}^3$.

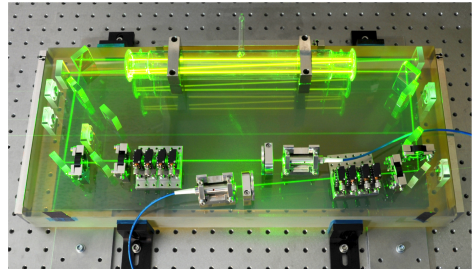


Figure 15: Photograph of the EBB spectroscopy setup.

Pump and probe beam are fiber-coupled to the board using polarization maintaining single-mode fibers with pigtailed fiber collimators (provided by OZ Optics Inc.). Both collimators are attached to ultra-stable invar mounts which enable the tilt adjustment using shims so that the parallelism of output beam and baseplate can be assured. The output beam diameter is 3 mm. Polarizers after the fiber output guarantee a clearly defined polarisation. Since all optic elements are directly joint to the baseplate four wedged AR-coated glass plates were placed in probe as well as in pump beam to have a possibility for adjustment of the two counterpropagating laser beams in the iodine cell. These wedges which are mounted in commercial rotation mounts allow an independent adjustment of both beams in two perpendicular directions. $\lambda/2$ plates and thin film polarizers (TFP) are used to control the optical power on the detectors (NC reference beam, RAM detector). A reference beam is led to the NC using a thin film polarizer. The other parts of the beams pass $\lambda/2$

plates again so that they can be led to glass plates which split of another part for intensity stabilisation. Subsequently, both beams pass the iodine gas cell thrice. The probe beam is outcoupled at a TFP towards a noise-cancelling detector for generating the error signal whereas the pump beam is dumped. In order to focus the laser beams onto the photo diodes of the detectors we adhesive bonded fused silica substrates to the baseplate which are provided with lenses.

Optical frequency reference on EM-level

In a following activity, a spectroscopy setup on engineering model (EM) level was realized, based on the experience gained with the EBB setup. The EM setup is further developed with respect to compactness and thermal and mechanical stability. It utilizes a $380 \times 180 \times 40 \text{ mm}^3$ baseplate and a compact $100 \times 100 \times 100 \text{ mm}^3$ multi-pass gas cell in nine-pass configuration. For high mechanical stability, an alternative cell cooling design was realized. Optical components (mirros, beam splitter, thin film polarizers) as well as the gas cell and the baseplate are made out of fused silica in order to ensure small differential CTE and therefore high mechanical and thermal stability. Commercial fiber launchers are placed in mounts made of Invar, waveplates and polarizers are mounted to holders made of titanium for CTE matching. As in the EBB, the optical components are integrated using adhesive bonding technology. Beam parameters and cooling finger temperature are similar to the EBB setup as described above.

Beside the EBB laser system, an additional light source was realized using an NPRO type Nd:YAG laser with external fiber-coupled frequency doubling waveguide modules. As in the EBB, intensity and RAM stabilization using two AOMs was implemented. A CAD model of the EM spectroscopy unit is shown in Fig. 16, a photograph of the integrated EM in Fig. 17.

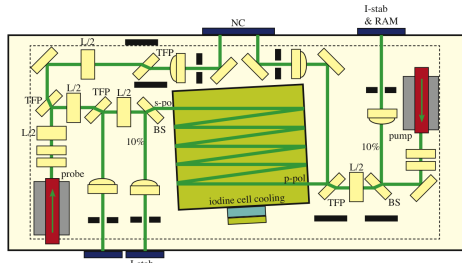


Figure 16: Schematic of the spectroscopy setup on EM level. NC: noise-cancelling detector; RAM: Residual Amplitude Modulation (caused mainly by the electro-optic modulator); TFP: thin film polarizer; BS: beam splitter; L/2: lambda/2 waveplate.

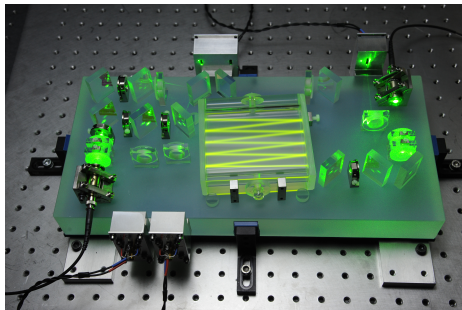


Figure 17: Photograph of the spectroscopy unit on engineering model (EM) level.

The EM setup was subjected to environmental testing including thermal cycling (8 cycles, -20°C to $+60^\circ\text{C}$) and vibrational testing (30 g sinus vibration and up to $25.1 \text{ g}_{\text{rms}}$ random vibration). The performance was checked before and after testing, where no degradation in frequency stability was observed.

First frequency stability measurements by beating the two iodine standards and a ULE cavity were performed at the Humboldt-University Berlin (HUB). The results, given in Allan deviation, are shown in Fig. 18.

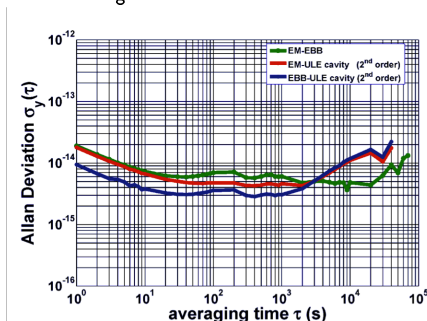


Figure 18: Measurements of frequency stability by beating the two iodine frequency references (on EBB and EM level) and a ULE-cavity. A frequency stability better than $4 \cdot 10^{-15}$ at an integration time of 200 s was demonstrated. For the cavities, a second order drift was removed.

This work was supported by the German Space Agency DLR with funds provided by the Federal Ministry of Economics and Technology (BMWi) under grant numbers 50QT1201 and 50QT1102.

An ESA-candidate mission: SpaceTime Explorer and Quantum Equivalence Principle Space Test

Thilo Schuldt, Markus Oswald, Johannes Stühler, Matthias Franz, and Claus Braxmaier

The Space-Time Explorer and Quantum Equivalence Principle Space Test mission (STE-QUEST) was selected by ESA as one of four candidates for the M3 mission within the Cosmic Vision Program with launch in 2022. The satellite will host an atom interferometer and a microwave link, optionally an optical clock and a laser link. Currently, an assessment study for the STE-QUEST atom interferometer is carried out on behalf of the German Aerospace Agency DLR where the first phase of the study is led by HTWG Konstanz. This study includes partners at the Leibniz-University Hannover, Humboldt-University Berlin, University Bremen/ZARM, University Hamburg, DLR institute of space systems Bremen and Airbus Defence and Space (Friedrichshafen, formerly Astrium GmbH) and is embedded in a European ESA coordinated activity including Germany, France, Great Britain and Italy.

The STE-QUEST (Space-Time Explorer and Quantum Equivalence Principle Space Test) satellite will host an atomic clock and an atom interferometer operated with the same atomic species, Rubidium-87 (^{87}Rb). A second atom interferometer with a different isotope of the same species, Rubidium-85 (^{85}Rb), will be operated as reference. STE-QUEST will test the far reaching consequences of Einstein's postulate and one of the most fundamental predictions of Einstein's Theory of General Relativity with high precision. It thereby searches for hints of quantum effects in gravity, contributing to the exploration of one of the current frontiers in fundamental physics. The mission will measure space-time curvature via the precise determination of gravitational time dilation, i.e. the difference in the ticking rate of the satellite's atomic clock when it is compared with a ground-based clock. At the same time, the satellite will allow for the comparison of the free propagation of coherent matter waves of ^{85}Rb and ^{87}Rb under the influence of the Earth's gravity with precision matter wave interferometry, striving for an accuracy of few parts in 10^{15} and beyond. The use of ultra-cold matter at quantum degeneracy will permit to go far beyond the current accuracy of quantum tests.

A highly elliptic orbit of the satellite is foreseen for STE-QUEST, providing a large variation in the gravitational potential between perigee and apogee and maximizing the accuracy of the measurements of the redshift. A mission duration of up to 5 years is intended. A sketch of the STE-QUEST mission concept is shown in Figure 19. During apogee, the STE-QUEST atomic clock is

compared to one or more ground based clocks, during perigee, the local acceleration of the two Rb isotopes is measured and compared via atom interferometry.

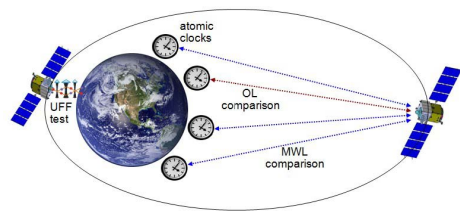


Figure 19: Sketch of the STE-QUEST mission concept using a highly elliptical orbit.

The STE-QUEST dual atom interferometer payload, which is based on the strong European developments in this field, is measuring the differential acceleration of the two atomic Rubidium isotopes along one axis with respect to the spacecraft with a resolution of 10^{-12} m/s^2 . The high common mode rejection of the dual atom interferometer permits to achieve this high differential accelerational resolution despite the ambient vibrational noise of the spacecraft. For achieving an optimal suppression of common-mode-noise, which accords to basically all possible sources of disturbance, the two atomic species are simultaneously prepared, coherently manipulated and detected with optimally overlapped atomic clouds of the two species.

A sketch of the STE-QUEST satellite is shown in Figure 20. The instrument payload is the central part of the spacecraft and includes the atomic

clock and the atom interferometer, cf. Figure 21.

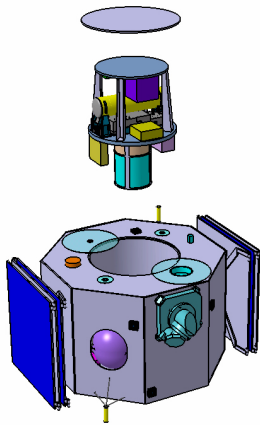


Figure 20: Sketch of the STE-QUEST satellite with the central payload accommodation.

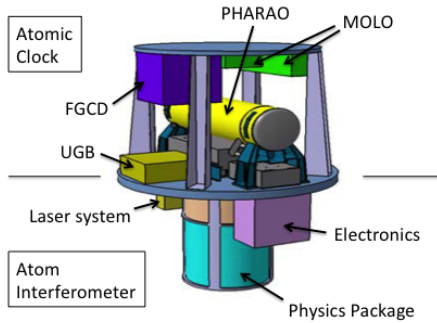


Figure 21: Sketch of the STE-QUEST instrument assembly containing the atomic clock and the atom interferometer. MOLO: Microwave-Optical Local Oscillator; PHARAO: Rb-based microwave atomic clock; FGCD: Frequency Generation, Comparison and Distribution unit; UGB: on-board management unit.

The key parameters of the atom interferometer are the atom number of 10^6 , a free evolution time between beam splitter pulses of 5 s, and a resulting repetition rate of 20 s. With these parameters the single shot precision at the shot noise limit will be $2.5 \cdot 10^{-12}$ and the target sensitivity at the 1^{-15} level will be reached after integration over 635 days.

The atom interferometer consists of a physics package, a laser system and the corresponding control electronics. The physics package includes the coherent matter wave source, an atom chip combined with a dipole trap, the beam splitter unit, and the detection system. The laser system

comprises the laser sources for laser cooling and trapping, state preparation and detection as well as the coherent manipulation of the atoms for forming the interferometer. In addition the system includes the laser for confining the atoms in a dipole trap. The laser system also includes the light distribution module for modifying and controlling the laser frequency, polarisation and power. The control electronics consists of a data management unit, a low noise RF generator, and several driver modules to control the laser system and physics package. A CAD preliminary design of the atom interferometer physics package is shown in Figure 22. Figure 23 gives an overview over the science chamber housing the atom chip at its center. The different optical accesses for interferometry, atom preparation, detection and manipulation are detailed.

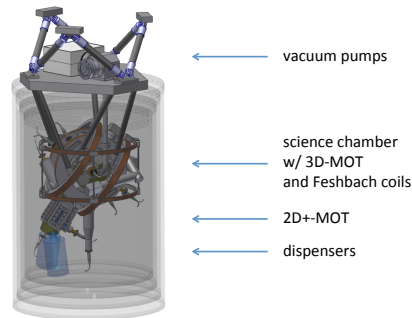


Figure 22: Preliminary design of the dual species atom interferometer physics package.

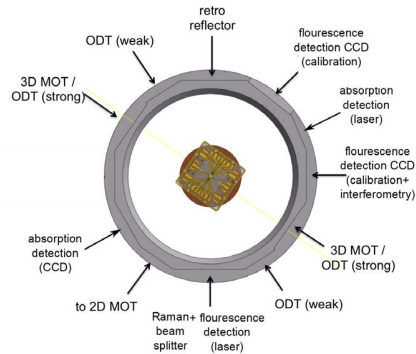


Figure 23: Schematic view of the science chamber of the atom interferometer. Detailed are the different optical ports for interferometry (Raman beam and retro reflector), detection (fluorescence and absorption), optical dipole trap (ODT) and 3D-MOT (magneto-optical trap).

The assessment phase was finalized end of 2013, resulting in a preliminary design of the atom interferometer payload and a full description of the experiment outline including a detailed error analysis.

Double Reflector Luminaire with homogeneous rectangular light distribution

Arnold Allweier and Bernd Joedicke

We present the design of a double reflector LED luminaire. By shaping the light with two different mirrors we achieved an almost perfect rectangularly illuminated surface. It could thus be shown almost any desired shaping of light is possible by using double reflector technique.

Introduction

LED-light sources have a high luminance and small surface. Thus it is possible to shape the light beam as desired. It is well known pointlike light sources are used in focussing luminaires. However using LEDs for precisely illuminating a spread surface area has not often been addressed. We have shown in 2010 that highly efficient and accurate lighting using a double reflector LED luminaire can be achieved.

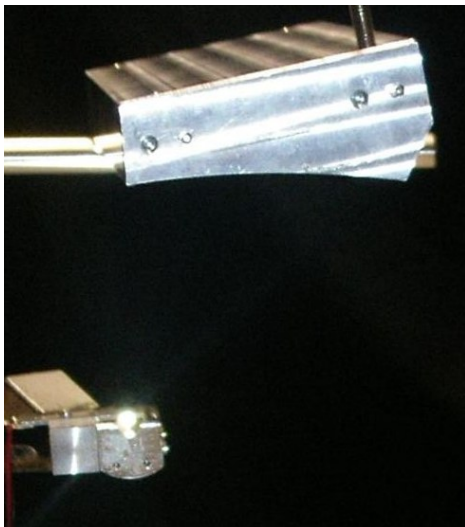


Figure 24: double reflector luminaire detail

A surface in our HTWG lighting-lab was illuminated with a uniform, perfectly rectangular illuminance distribution. The results are summarized. The luminaire itself consists of two reflectors. The first nut-like shape reflector restricts the lateral amount of light. The second parabolic groove distributes the light evenly upon the underlying surface. The reflectors' shapes have been optimized using forward-raytracing-simulation.

Experimental Setup

In order to be able to proof the principle of the access, the street lamp was manufactured in a 1:5 scale. One high power LED and two reflectors were used. The LED shines down into the first nut-like reflector. The light then reaches the above mounted parabolic groove reflector, which in its turn illuminates the floor. Using this setup almost all lumious flux produced by the LED is collected in the reflectors.

The whole setup was tested in the light-lab at the UAS Constance. In the dark-room the illuminance underneath the luminaire was evaluated, measuring it step by step using a lux-meter. The room itself had to be perfectly dark, since the luminous intensity of only one LED was quite small.

Measuring the illuminance distribution on the floor shows the very homogeneous behavior. The dark area underneath the luminaires results from the shadow of the LED support. This is due to the fact that the luminaire only consists of one single LED. If more LEDs are used this shadow will disappear.

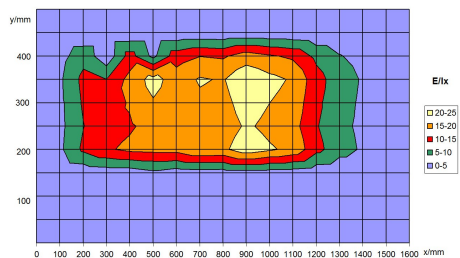


Figure 25: Illuminance distribution



Figure 26: Lighted area underneath the setup

Results

The illuminance distribution in the ground is almost perfectly rectangular and very homogeneous as can be seen in fig. 3. The illuminated surface lies between 150 mm and 1400 mm, and has a width of 25 mm. It expands in exactly the same light distribution also to negative values. The illumination below the luminaire (which is located at $x=0$; $y=0$) is close to zero due to the shadow thrown from the luminaire's first reflector.

Numerically integrating the illuminance of the lighted rectangular area results in a luminous flux of 9,5 lm. The LED is driven by a power of 0,23 W and has a luminous efficacy of approximately 60-70 lm/W. This results in a luminaire's efficiency of over 60%. This is a decent value, but it should however not be overemphasized, since the luminaire model was not optimized to high efficiency. Using better reflector material will further improve the luminaire significantly.

Light distribution

Calculating the achieved luminous intensity results in an almost perfect distribution needed for street

lights.

The light produced by the LEDs is spread homogeneously to both sides of the lantern. The luminaire also spreads its light in a forward direction, namely the direction of the road.

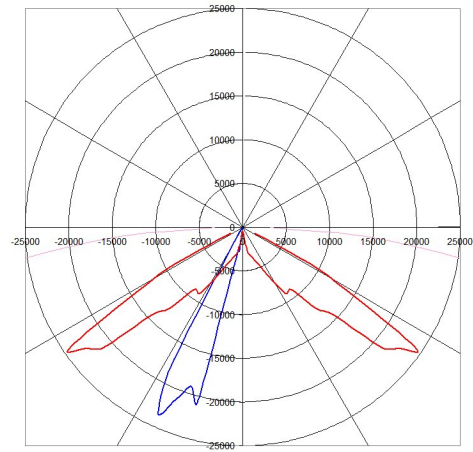


Figure 27: Luminous intensity distribution

Summary and next steps

We have shown by using an optimized double reflector system, a uniformly distributed, rectangular illumination of a street is possible. It has been proven on a laboratory scale, with a high luminaire efficiency. The success is mainly due to the LEDs high luminance. This can be used to shape light ray distribution according to the needs.

In further steps the concept should be applied to full-scale street lamps.

Picometer and Nanoradian Heterodyne Interferometry

Hanna Wenzl, Jan Benz and Bernd Joedicke

We present the reconstruction of a measuring setup which allows to specify the luminous efficacy of a LED by determination of installed luminous flux subject to the operating temperature and the electrical power supplied.

Introduction

The luminous efficacy describes the ratio of lamp's luminous flux to the electric power supplied. It establishes a relation between the physiological unit of installed lamp luminous flux which includes the responsivity of human eyes and the physical unit electrical power. The total installed luminous flux can be determined with an Ulbricht sphere. The light output, but also the efficacy of a light source is dependent on the applied voltage, electrical current and operating temperature. Luminous flux and electrical currents are recorded at different operating temperatures. The applied voltages are also measured. The total luminous flux of the LED comprises of illuminance detected by the sensor of the Ulbricht sphere and a correction factor c determined by calibration. The luminous efficacy of the LED at each operating temperature can be determined by the luminous flux and the electrical power applied by the following formula:

$$\eta(T) = \frac{\phi(T)}{P_{el}} = \frac{I_{\text{Sensor}} \times c}{I_{\text{LED}} \times U_{\text{LED}}}$$

Experimental Setup

For calibrating the whole Ulbricht sphere setup, including the sensor, the opening of the sphere is illuminated by calibration lamp is measured from a distance of 50 cm. The installed luminous flux can be determined by the diameter of the opening of the Ulbricht sphere, the sensors relative luminous sensitivity and the data from the calibration certificate.

$$\phi = K \times \sum V(\lambda) \times I(\lambda) \times \Delta\lambda$$

A sensor specific absolute term c can be calculated. It enables the conversion of measured illuminance into luminous flux.

$$c = \frac{\phi}{I_{\text{Sensor}}} [= 0,6192 \frac{\text{lm}}{\mu\text{A}}]$$

The above mentioned factor c is preliminary due to the uncertainty of a spectral response of the sensor.

The temperature control is realized by two controllers and a Peltier element. A copper conductor is used as heat buffer to prevent severe heat fluctuations and offers a possibility to install the temperature sensor. The LED is mounted onto the conductor with heat conductor pads. The temperatures reached are measured with a sensor and stored in a data logger.

The LED is fixed with a bezel to the integrating sphere so that no light can diffuse out of the sphere. The illuminance is measured with a Dual Channel Optometer.

Result

The maximum luminous efficacy of 16,5 lm/W is reached at a power of 0,27W. It decreases to 6,04 lm/W at 3,3W which is a degradation of 64%. One can observe a massive decline of luminous efficacy over electrical power. Furthermore, it is found that the higher the temperature the less luminous efficacy and the higher the electrical power the less luminous efficacy. According to solid-state physics theory higher temperature within a solid lead to more inefficient the generation of light. This is in accordance with our measurement. High electrical power leads to high losses within the solid which are apparently far more important than the temperature variations applied from the outside. The luminous efficacy tends to decrease linear with increasing temperature. An exception to this is the test series at 100 mA. The slope of the trend lines varies from 0,0163 to -0,0435 lm/(W*K). Considering the effect of a tenfold increase in applied electrical power one can only observe an approximately four times higher luminous flux.

For low electrical power, the applied temperature has almost none to the point of a slightly positive effect on luminous efficacy. At higher electrical powers an increase in temperature leads to losses in efficacy. One can clearly identify that temperature influences luminous efficacy but the electrical power at which the LED is operated impacts the efficacy far more.

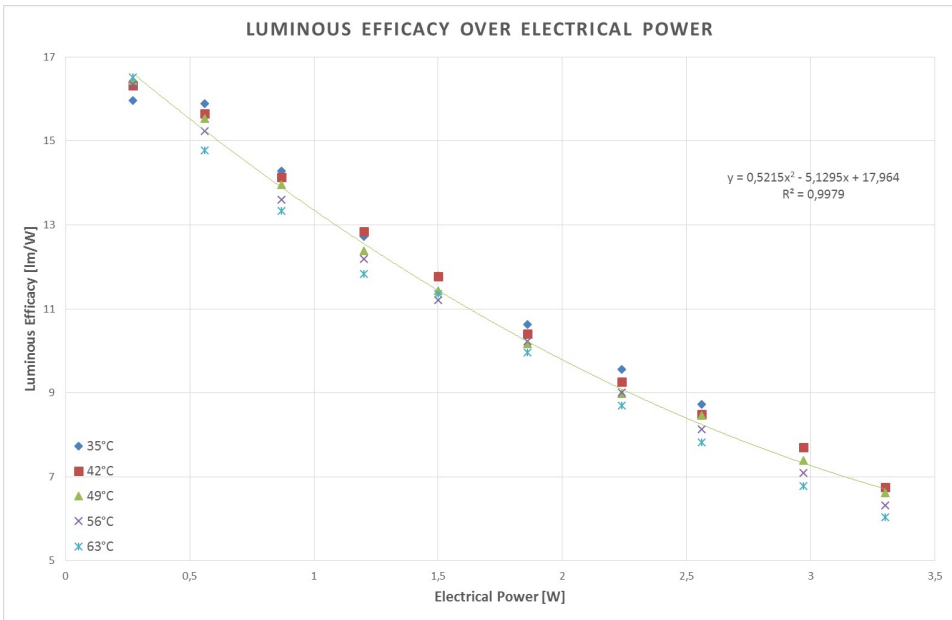


Figure 28: Luminous Efficacy over Electrical Power

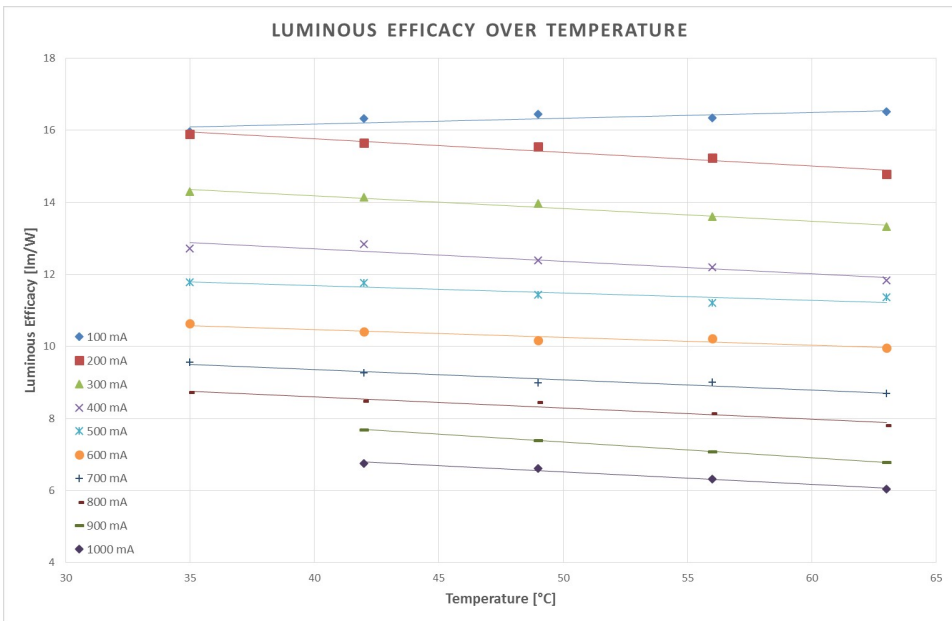


Figure 29: Luminous Efficacy over Temperature

Attempt of an empirical theoretical classification

The luminous efficacy is a function of the temperature at the light generating PN junction. The temperature at this point can be increased in two ways: by increasing the outside temperature or by increasing electrical losses. There is a limit temperature to which the luminous efficacy is practically unaffected by temperature. Once this temperature is passed there is a linear correlation between luminous efficacy and temperature.

The maximum measured luminous efficacy reaches a level far below expectations. In order to rule out errors in measurement and in test setup we perform a plausibility check.

A 50W light bulb with an installed luminous flux of 710 lm is measured in the existing test setup. The luminous flux can be determined with the il-

lumination level and the diameter of the Ulbricht sphere. The reassessed constant c only differs from the original c by five percent. Therefore serious errors in measurement and in test setup can be ruled out. Nevertheless the influence of the sensor's spectral response can not be eliminated within this project. This leads to the result that the data should not be trusted in absolute values. However comparing efficacy considerations may be regarded as being correct.

Next Steps

The calibration factor accuracy has to be critically analyzed with special regard to the sensor's spectral response. Furthermore the temperature control and regulation should be improved since slight problems occurred time and again. Apart from that the measuring setup is fully operational and can be used to analyze any other LED.



ios konstanz
htwg konstanz
brauneggerstr. 55
78462 konstanz
www.ios.htwg-konstanz.de